Indian Journal of Biochemistry & Biophysics
Vol. 61, April 2024, pp. 204-222
DOI: 10.56042/ijbb.v61i4.8236

Docking studies, molecular structure, and spectroscopic analysis of 3-chlorobenzamide as an anti-cancer agent

N Karthik, S Jeyavijayan* & S Sumathi

Department of Physics, Kalasalingam Academy of Research and Education, Krishnankoil-626 126, Tamil Nadu, India

Received 22 January 2024; *revised 08 February 2024*

In this study, the FTIR and FT-Raman spectroscopies have been used to analyze the vibrational spectral characteristics of 3-chlorobenzamide (3CBA). Density functional theory (DFT) with B3LYP method has been used for theoretical computations, a number of solvents and diffuse functions (6-311+G(d,p) and 6-311++G(d,p)) have been used. The determined vibrational frequencies and structural parameters have been examined and compared with the experimental data. To clarify the electronic characteristics of the molecule, computations have been made using the frontier molecular orbital (FMO), molecular electrostatic potential (MEP), Fukui function and Mulliken analysis. The theoretical UV-Vis spectral study using various solvents (methanol and ethanol) has been made using time-dependent DFT computations. Molecular orbital contributions are investigated by densities of states (DOS) spectrum. The NMR chemical shifts for ^{1}H and ^{13}C have been computed using the gauge-independent atomic orbital technique. From the docking analysis of the molecule, the ovarian cancer inhibitors (human Matrix metalloproteinase-2) showed the binding affinity of -6.5 and -6.4 kcal/mol, and breast cancer inhibitors (human progesterone and allosteric inhibitor) showed the binding affinity of -6.0 and -5.7 kcal/mol, which are comparable with the binding affinity of standard drugs. To reveal the drug similarity, ADMET prediction has been utilized. Thus, the molecule's computational and biological properties show that it is a promising therapeutic candidate for the treatment of both ovarian and breast cancers.

Keywords: 3-chlorobenzamide, Breast cancer, DFT, Docking, Fukui function, Ovarian cancer

Amide is referred to as a peptide bond when it appears in a protein's main chain and as an iso-peptide bond when it occurs in a protein's side chain. N-alkyl amides found in plants are biologically active and useful in medications, including penicillin[1]. Benzamide is the most fundamental aromatic carboxylic amide, and its derivatives have a variety of pharmacological effects, such as reducing pain and having antibacterial, anti-inflammatory, anticancer, cardiovascular, and other biological qualities[2]. Its compounds are useful therapeutically for treating obesity-related illnesses and cancer. It has been demonstrated that their derivatives inhibit the growth of malignant cells[3]. For benzamides, in vitro antibacterial bustle has been demonstrated and the antimicrobial activity against Staphylococcus aurous is most effective[4]. Recently, a number of scientists have studied the molecular structure of derivatives of benzamides using spectroscopy and computational methods[5,6]. Furthermore, numerous studies have been explored the anti-cancer efficacy of benzamide derivatives[7,8]. A thorough review of the literature revealed that 3-chlorobenzamide (3CBA) has yet to be the subject of considerable theoretical and experimental investigation. This has been explained both theoretically and empirically using FT-Raman and FTIR spectra. Spectroscopic data acquired experimentally was confirmed by DFT simulations[9,10]. One of the most useful DFT computationsis the Lee Yang and Parr (LYP) connection functional, which recovers energetic electron linkages and Becke's 3 parameter (B3) exchange-correlations[11]. They are useful when you have a system with large electron density like halogen ions/electronegative elements or radicals and solvation in DFT calculations. This study stimulates the supply of spectroscopic and substantial theoretical research employing two distinct basis sets such as6-311+G(d,p) and 6-311++G(d,p) (the notation + or ++ represent diffuse functions on heavy elements (*i.e.* other than hydrogen) and on hydrogen and heavy atoms). Hence, the DFT/B3LYP has been used to analyze electronic transitions inside the molecule 3CBA using molecular reactivity factors including frontier molecular orbital analysis and MEP surface analysis. Total DOS spectrum of 3CBA can

*Correspondence:
E-mail: sjeyavijayan@gmail.com

provide the description of all frontier molecular orbitals. The electronegativity, chemical softness, hardness, and electrophilicity index of 3CBA have all been determined[12]. The 3CBA molecule's natural bond orbitals have been shown to identify the inter and intramolecular interactions of the compound. In addition, the 3CBA's Fukui function values and Mulliken analysis have been computed. The gauge-independent atomic orbital technique has been used to determine the NMR shifts for ^{1}H and ^{13}C for 3CBA. The therapeutic molecule 3CBA's pharmacological characteristics and binding affinity with ovarian cancer and breast cancer inhibitors have been determined by docking analysis[13,14] and these results are equivalent to the binding affinities of conventional medications. ADMET experiments are being conducted to evaluate 3CBA's biological potential.

Materials and Methods

Experimental characterizations

For the spectral measurements, a fine polycrystalline sample of 3CBA was employed, which was provided by Sigma Aldrich, UK, for the spectrum investigations. Sample was compressed into a KBr pellet after being reduced to a powder. The 3CBA molecule's FTIR spectrum at ambient temperature was acquired in the range 4000–400 cm^{-1} at a resolution of ±1 cm^{-1} using a BRUKER IFS 66V model FTIR spectrometer with an MCT detector, KBr beam splitter, and globar source. The FT-Raman spectrum of 3CBA was acquired using a computer-interfaced BRUKER IFS 66V type interferometer outfitted with FRA-106 FT-Raman accessories. The spectrum was measured in the Stokes region (4000-50 cm^{-1}) using a Nd:YAG laser with a 200 mW output at 1064 nm and a liquid nitrogen-cooled Ge-diode detector. The powder sample was in a capillary tube. 1000 scans were gathered to improve the signal-to-noise ratio, with a total registration time of around 30 min. The quoted wave numbers are believed to be accurate within ±1 cm.

Quantum computational details

Theoretical approaches and basis sets should be explored to fulfill the needs of both accuracy and computational economy. DFT has proven to be quite effective in handling molecular electronic structures. The Gaussian 09 suite programme package[15] was used to determine the vibrational harmonic frequencies and molecular structure optimization of the 3CBA molecule using DFT with Becke-3-Lee–Yang–Parr (B3LYP) in combination with normal 6-311+G(d,p) and 6-311++G(d,p) basis sets. The structural parameters of 3CBA have been optimized before computing chemical shifts, electronic properties, and vibrational wavenumbers. The vibrational wavenumbers have been calculated by merging the results of the GAUSSVIEW[16] and VEDA[17] algorithms. The vibrational frequency calculations of 3CBA have been used to evaluate changes in thermodynamic functions (vibrational energy, entropy and heat capacity). The time-dependent DFT method has been used to calculate the energy of vertical excitation, electronic transitions, oscillator strengths, and absorbance. The chemical activity of 3CBA has been found by computing its electrostatic potentials (MEP), HOMO and LUMO energies, and reactive sites in gas phase, methanol, and ethanol solvations. Since the second order interactions between the full orbitals of one subsystem and the empty orbitals of another subsystem are measured by intermolecular delocalization, NBO calculations have been performed. The most widely used technique for calculating nuclear magnetic shielding tensors is the GIAO method[18], which yields the ^{13}C and ^{1}H NMR chemical shifts. In addition to these calculations, the GaussSum[19] has been used to create TDOS spectra, and the charge contribution to every atom in the molecule has been estimated through the use of Mulliken population study.

Molecular docking and ADMET

The progesterone and inhibitor receptors trigger several cellular downstream signaling pathways, which leads to the development and spread of cancer. To ascertain 3CBA's inhibitory effectiveness on ovarian and breast cancer receptors, we utilized a computer-based molecular modeling method. Protein markers for ovarian cancer such as human Matrix metalloproteinase-2 (MMP-2) receptors (PDB ID: 7XJO and PDB ID: 7XGJ) and markers for breast cancer like human progesterone (PDB ID: 4OAR) and allosteric inhibitor (PDB ID: 5KCV) receptors have been identified using 3CBA as a ligand. The molecular docking procedure has been performed using Auto Dock Vina[20] (Version: 4.2.1), and with PyMOL molecular graphical system[21] (Version 1.7.4.5 Edu), the protein-ligand binding location has been shown. Prior to molecular docking, the protein structure and amino acid positions have been analyzed using Discovery Studio[22] (Version: 2017 R2 client). One of the public ligand databases, PubChem

(http://pubch em.ncbi.nlm.nih.gov), has been utilized to derive the structure of the ligand 3CBA. Using the ADMET-SAR prediction program[23] (http://lmmd.ecust.edu.cn/admetsar2/) to evaluate the ADMET (Adsorption, Distribution, Metabolism, and Toxicity) predictions of 3CBA, the pharmacodynamic effects in the human body have been supported.

Results and Discussion

Molecular geometry analysis

Table 1 presents the optimal values of 3CBA based on the atom numbering method depicted in (Fig. 1).

Table 1 — Optimized structural parameters of 3-chlorobenzamide

Bond length (Å)	Structural parameters		
	6-311+G(d,p)	6-311++G(d,p)	Experimental[24]
C1-C2	1.3991	1.3991	1.392
C1-C6	1.3979	1.3979	1.389
C1-C12	1.5058	1.5058	1.491
C2-C3	1.3906	1.3906	1.378
C2-H7	1.0825	1.0825	0.95
C3-C4	1.3909	1.3909	1.380
C3- Cl8	1.7593	1.7593	1.7386
C4-C5	1.3944	1.3944	1.388
C4-H9	1.0825	1.0825	0.95
C5-C6	1.3905	1.3905	1.383
C5-H10	1.0838	1.0838	0.95
C6-H11	1.0824	1.0825	0.95
C12-O13	1.2192	1.2193	1.2216
C12-N14	1.3709	1.3709	1.3696
N14-H15	1.0089	1.0089	0.94
N14-H16	1.0067	1.0067	0.94
Bond angle (^{0})			
C2-C1-C6	119.68	119.68	119.59
C2-C1-C12	122.63	122.63	124.15
C6-C1-C12	117.66	117.66	116.03
C1-C2-C3	119.35	119.35	119.46
C1-C2-H7	121.40	121.40	120.2
C3-C2-H7	119.20	119.20	120.2
C2-C3-C4	121.40	121.40	121.49
C2-C3-Cl8	119.16	119.16	118.93
C4-C3-Cl8	119.42	119.42	119.52
C3-C4-C5	118.84	118.84	118.48
C3-C4-H9	120.09	120.09	120.8
C5-C4-H9	121.05	121.04	120.8
C4-C5-C6	120.58	120.58	121.08
C4-C5-H10	119.39	119.38	119.5
C6-C5-H10	120.02	120.02	120.5
C1-C6-C5	120.11	120.11	119.71
C1-C6-H11	118.58	118.59	120.1
C5-C6-H11	121.29	121.29	120.1
C1-C12-O13	121.64	121.64	121.46
C1-C12-N14	116.36	116.35	117.86
O13-C12-N14	121.98	121.98	120.63
C12-N14-H15	116.35	116.34	111.8
C12-N14-H16	121.43	121.42	122.53
H15-N14-H16	117.43	117.43	111.8

These parameters have been computed using B3LYP method by different diffuse functions (6-311+G(d,p), 6-311++G(d,p)) and are compared with the experimental data[24]. In both functions, all of these optimized parameters are almost identical. Some of the expected attributes are found to deviate considerably from the observed values since the theoretical calculations relate to a gaseous phase molecule whereas the experimental data concerns a solid-state molecule. The 6-311+G(d,p) and 6-311++G (d,p) functions have local minimum energies of -860.69224421 and -860.6923884, respectively.

The seven C-C bonds, four C-H bonds, two N-H bonds, and one each of C-Cl, C-O, and C-N bonds make up this molecule. For 3CBA, the C-H bond lengths are altered from 1.0824 to 1.0838 Å. The C-C bond distances are extended from 1.3905 to 1.5058 Å using the B3LYP/6-311++G(d,p) technique, which is in line with the reported experimental XRD (1.383-1.491Å). The bond lengths of C3–Cl8 is 1.7593 Å, complied with experimental value 1.7386 Å, which is larger than any other bond distances of 3CBA. This demonstrates unequivocally that the π-electrons around this connection have not delocalized. The DFT approach in 3CBA yields the bond lengths of N14-H15, N14-H16, and C1-C12 as 1.0089, 1.0067, and 1.5058 Å, respectively. These values correspond well with the 0.94, 0.94, and 1.491 Å from the experimental results. The calculated bond length for C12-O13 is found to be 1.2193 Å which is also complied with experimental value (1.2216 Å).The C2-C1-C12 bond angle (122.63°) is

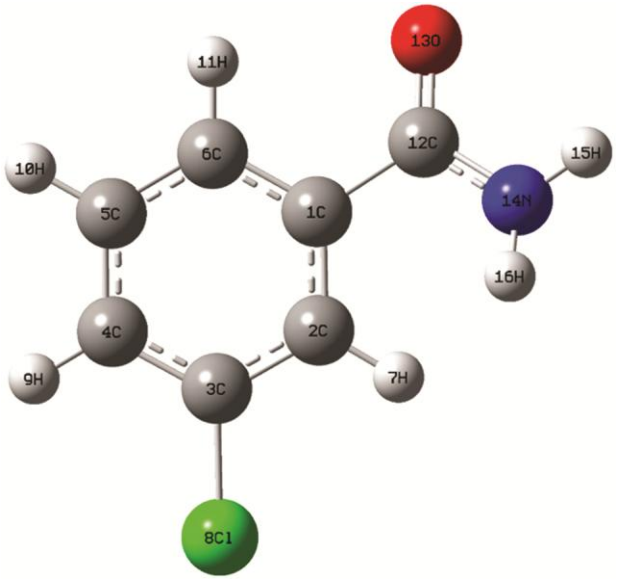

Fig. 1 — Optimized structure of 3-chlorobenzamide

higher than the other C-C-C angles because the electronegative oxygen (O13) atom is connected at C12. For C2-C3-C4, C1-C12-N14,C3-C4-H9, C2-C3-Cl8, and O13-C12-N14, the bond angles obtained from DFT calculations are 121.40°, 116.36°, 120.09°, 119.16°, and 121.98° (corresponding experimental values: 121.49°, 118.93°, 120.8°, 117.86°, and 120.63°).

The thermodynamic parameters (dipole moment, thermal energy, entropy, specific heat capacity, rotational constants, and including zero-point vibrational energy) of 3CBA has been investigated using the DFT/B3LYP 6-311+G(d,p) and 6-311++G(d,p) technique and are shown in (Table 2). The molecule 3CBA has a greater dipole moment of 2.2947 and 2.2891 Debye because it contains highly electronegative nitrogen, oxygen and chlorine atoms. The overall energy of 3CBA is determined to be 79.186 and 79.165 kcal mol^{-1} and entropy of 3CBA is found to be 93.390 and 93.394 cal $mol^{-1}k^{-1}$ at two diffuse functions. At 73.66920 and 73.64658 kcal mol^{-1}, the immaterial vibrational energy (zero-point) is reached for 3CBA. The assessment of chemical reactions of 3CBA can be done with the help of these thermodynamic parameters.

Vibrational assignments

The 16 atoms of 3CBA have 42 normal modes of vibrations. Using DFT/B3LYP/6-311+G(d,p) and 6-311++G(d,p) approaches, the thorough vibrational assignments are described for 3CBA. Due to a combination of electron correlation effects and basis set faults, the calculated frequencies are greater than the corresponding experimental frequencies. Here, the scale factor[25] of 0.9613 from the B3LYP approach is used to correctly scale the calculated wavenumbers. Table 3 presents a comparison of the vibrational frequencies obtained for 3CBA by theoretical and experimental methods (FTIR and FT-Raman). Figures 2 and 3 show the observed FTIR and FT-Raman of 3CBA, respectively.

Table 2 — The thermodynamic parameters of 3-chlorobenzamide

Parameters	DFT-B3LYP/ 6-311+G(d,p)	DFT-B3LYP/ 6-311++G(d,p)
Optimized global minimum Energy (Hartrees)	-860.69224421	-860.6923884
Total energy(thermal),E_{total} (kcal mol^{-1})	79.186	79.165
Heat capacity, C_v (cal mol^{-1} k^{-1})	33.148	33.168
Total Entropy, S (cal mol^{-1} k^{-1})	93.390	93.394
Translational Entropy (cal mol^{-1} k^{-1})	41.025	41.025
Rotational Entropy (cal mol^{-1} k^{-1})	30.345	30.345
Vibrational Entropy (cal mol^{-1} k^{-1})	22.021	22.025
Vibrational energy, E_{vib} (kcal mol^{-1})	77.409	77.388
Zero-point vibrational energy, (kcal mol^{-1})	73.66920	73.64658
Rotational constants (GHz)		
A	2.20791	2.20793
B	0.69681	0.69685
C	0.53622	0.53621
Dipole moment (Debye)	2.2947	2.2891

N-H vibrations

The amide group possesses six normal modes: four bending vibrations, which include twisting, rocking, wagging, and scissoring modes, and two stretching vibrations, which include symmetric and asymmetric stretching modes. In general, the N-H stretching vibrations[2] in primary amines occur in the range of 3500-3300 cm^{-1}. In this instance, the asymmetric stretching vibration of 3CBA is estimated to be 3569 cm^{-1} and seen as very weak peak at 3567 cm^{-1} in FTIR spectrum. The NH_2 group's symmetric stretching vibration is calculated at 3449 cm^{-1} and found in the FT-Raman and FTIR spectra as very weak bandat 3400 cm^{-1} and strong band at 3360 cm^{-1}. Both of these modes may be considered as pure N-H stretching, as demonstrated by the PED data (almost 100%).

NH_2 groups' scissoring mode often manifests in the 1615–1650 cm^{-1} range. The NH_2 scissoring mode of 3CBA is calculated to be 1681 cm^{-1}, which closely matches the experimental data (medium strong band at 1684 cm^{-1} in FTIR and strong band at 1685 cm^{-1} in FT-Raman). The PED contribution of 70% to this assignment further supports the results. The FT-Raman spectrum revealed the NH_2 rocking vibration with a very strong band at 1000 cm^{-1} (85% PED), which is in close agreement with the estimated value of 1056 cm^{-1}. The NH_2 group's wagging mode of 3CBA is estimated to be 450 cm^{-1}, which closely matches with the experimental weak band at 460 cm^{-1} in FT-Raman.

C-H vibrations

The C-H stretching vibrations[2] of aromatic compounds and their derivatives are often not affected much by the kind of substituents, and these weak bands are frequently observed in the range of 3100–3000 cm^{-1}. As anticipated, the four C-H stretching vibrations of the 3CBA have been estimated at 3085, 3080, 3074, and 3058 cm^{-1}. The corresponding C-H stretching vibrations are found at 3175, 3100 cm^{-1} in Raman and at 3185, 3045 cm^{-1} in

Table 3 — Vibrational frequencies (cm^{-1}), IR intensities (Km mol^{-1}), Raman scattering activity ($Å^4$ amu^{-1}) and vibrational assignments based on PED calculations for 3-chlorobenzamide

S. No	Observed wave number (cm^{-1})		Calculated Wavenumber (cm^{-1})								Assignment with PED (%)
			DFT-B3LYP/6-311+G(d,p)				DFT-B3LYP/6-311++G(d,p)				
	FT-IR	FT- Raman	Un Scaled	Scaled	IR Intensity	Raman activity	Un Scaled	Scaled	IR Intensity	Raman activity	
1	3567 (vw)	-	3710	3567	40.4028	50.0928	3711	3569	40.4783	50.6028	NH_2 ass (100)
2	3360 (s)	3400 (vw)	3586	3447	46.0486	158.0225	3586	3449	45.7015	159.8063	NH_2ss (98)
3	3185 (ms)	-	3208	3084	3.1703	148.4541	3207	3085	45.7015	148.4989	νCH (97)
4	-	3175 (vw)	3202	3078	0.5234	85.7371	3202	3080	0.4798	85.1080	νCH (95)
5	-	3100 (ms)	3197	3073	0.5815	41.4015	3197	3074	0.5632	40.8445	νCH (96)
6	3045 (vw)	-	3179	3056	5.7347	79.3049	3179	3058	5.6495	79.8569	νCH (93)
7	1684 (ms)	1685 (s)	1748	1681	344.5842	44.3246	1748	1681	344.0328	44.2319	NH_2sciss (70)
8	1570 (ms)	1600 (s)	1633	1570	4.895	58.6274	1633	1571	4.8637	58.6389	νC=O (87)
9	-	1565 (vw)	1620	1558	136.0463	6.693	1620	1558	135.6368	6.7545	νCC (85)
10	-	1530 (vw)	1607	1545	65.1716	10.0049	1607	1546	65.2658	10.0239	νCC (86)
11	1440 (vw)	1450 (vw)	1506	1447	14.3909	2.7048	1506	1448	14.4874	2.6792	νCC (84)
12	1396 (vw)	1325 (vw)	1443	1387	10.1304	2.3615	1443	1387	10.1984	2.3580	νCC (82)
13	-	1300 (vw)	1357	1304	252.3435	25.1784	1357	1305	252.3033	25.5236	νCC (81)
14	1286 (vw)	1275 (vw)	1339	1287	1.5124	1.6749	1339	1287	1.5676	1.6774	νCC (80)
15	1264 (vw)	1250 (vw)	1302	1252	20.4098	2.9556	1302	1252	20.2771	2.9331	νCN (80)
16	1132 (ms)	1135 (w)	1189	1143	0.7104	2.2462	1189	1144	0.7076	2.3038	νCC (81)
17	1110 (vw)	-	1151	1106	33.1737	14.787	1151	1107	33.2042	14.6670	bCH (79)
18	-	1100 (vw)	1118	1075	4.1416	0.8343	1118	1076	4.1027	0.8561	bCH (78)
19	-	1000 (vs)	1098	1056	24.3755	13.2598	1098	1056	24.3452	13.1932	NH_2 rock (85)
20	1005 (vw)	-	1081	1039	12.0655	5.5433	1081	1040	12.1010	5.6138	bCH (77)
21	984 (vw)	-	1014	975	2.7823	40.7948	1014	975	2.7778	40.9236	bCH (76)
22	-	942 (vw)	1006	967	0.7499	0.3398	1001	963	0.7868	0.3590	R trigd (75)
23	896 (s)	-	942	906	0.4753	0.2168	940	904	0.6239	0.1162	R symd (74)
24	-	865 (vw)	903	868	9.5508	0.4244	898	864	8.8972	0.4825	bCN (75)
25	-	780 (vw)	824	792	17.3107	1.1485	824	793	17.7201	1.1690	R asymd (75)

(*Contd*.)

Table 3 — Vibrational frequencies (cm^{-1}), IR intensities (Km mol^{-1}), Raman scattering activity ($Å^4$ amu^{-1}) and vibrational assignments based on PED calculations for 3-chlorobenzamide (*Contd*.)

S. No	Observed wave number (cm^{-1})		Calculated Wavenumber (cm^{-1})								Assignment with PED (%)
			DFT-B3LYP/6-311+G(d,p)				DFT-B3LYP/6-311++G(d,p)				
	FT-IR	FT- Raman	Un Scaled	Scaled	IR Intensity	Raman activity	Un Scaled	Scaled	IR Intensity	Raman activity	
26	786 (ms)	-	819	788	19.4462	1.2725	819	787	18.5593	0.9244	bCC (74)
27	764 (ms)	712 (ms)	761	731	55.7213	0.3321	760	731	56.3887	0.3312	νCCl (72)
28	685 (vw)	-	697	670	10.788	2.6174	696	669	12.3165	4.2042	ωCH (64)
29	654 (vw)	650 (vw)	689	662	16.1465	7.9457	688	662	13.8130	6.3084	ωCH (63)
30	632 (vw)	-	628	604	22.0979	0.9191	628	604	22.1089	0.8489	ωCH (63)
31	588 (vw)	552 (vw)	568	546	19.9188	0.3784	569	547	20.5723	0.3248	ωCH (62)
32	504 (vw)	500 (vw)	529	509	4.6814	0.6315	529	509	4.6023	0.6294	bCCl (61)
33	-	460 (vw)	468	450	2.6887	0.3234	468	450	2.7252	0.4074	NH_2 wag (76)
34	-	412 (vw)	423	407	8.5575	2.1096	423	407	8.3071	2.0497	bC=O (71)
35	-	375 (vw)	400	385	6.6557	4.0245	400	385	6.6676	4.0388	ωCC (60)
36	-	362 (ms)	375	360	77.8694	4.4127	375	361	77.4181	4.4379	ωCCl (57)
37	-	350 (vw)	356	342	95.8318	0.8478	356	342	95.4656	0.8644	ωCN (60)
38	-	225 (s)	308	296	8.8996	3.3293	308	296	8.9998	3.2804	tRtrigd (62)
39	-	200 (s)	198	190	0.7117	1.3386	198	190	0.7103	1.2551	ωC=O (63)
40	-	150 (ms)	160	154	3.5886	0.9733	160	154	3.5850	0.9798	tRsymd (64)
41	-	-	137	132	3.806	1.9365	137	132	3.8331	1.9407	tRsymd (64)
42	-	-	53	51	10.6389	0.8533	53	51	10.6661	0.8719	NH_2 twist(60)

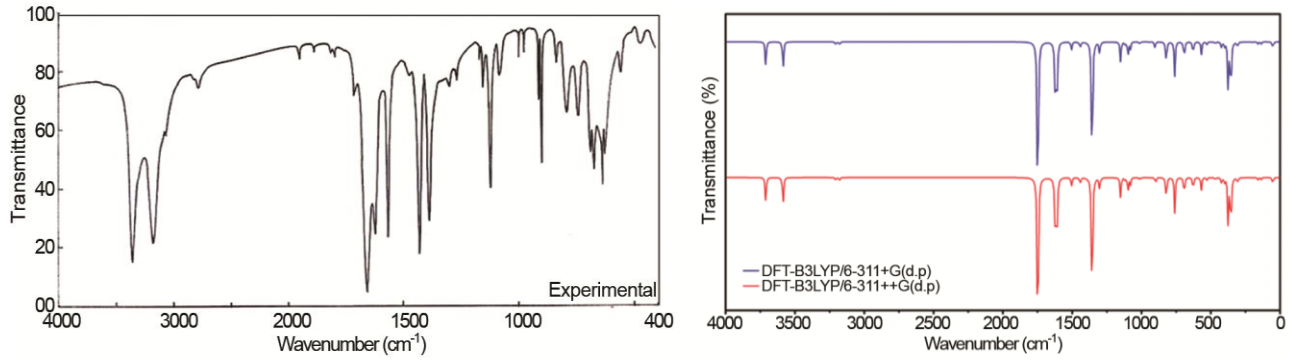

Fig. 2 — FTIR spectrum of 3-chlorobenzamide

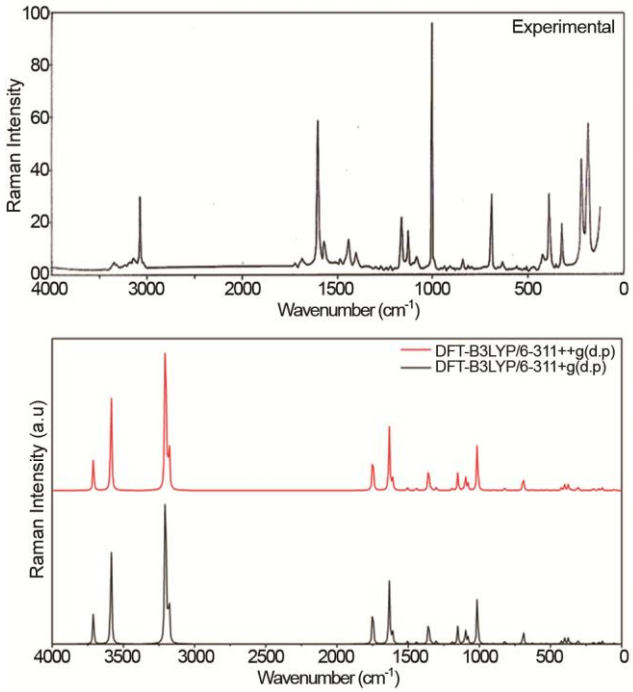

Fig. 3 — FT-Raman spectrum of 3-chlorobenzamide

FTIR. These modes almost provide 93-97% of PED, thus it's believed that they are pure stretching modes. The typical range for C-H in-plane bending vibrations in substituted benzene rings is 1500–1100 cm^{-1}, while the typical range for out-of-plane bending vibrations is 1000–700 cm^{-1}. The C-H in-plane bending modes are allocated to the FTIR bands set at 1110, 1005, 984, and 1100 cm^{-1}, as well as the FT-Raman at 1100 cm^{-1}. The equivalent theoretically scaled frequencies are 1107, 1076, 1040, and 975 cm^{-1}. The FTIR bands at 685, 654, 632, 588 cm^{-1} and the FT-Raman band at 650, 552 cm^{-1} are assigned for C-H out-of-plane bending vibrations of 3CBA which exhibit good agreement with the scaled B3LYP/6-311++G(d,p) results of 669, 662, 604, 547 cm^{-1}.

C-C and C-N vibrations

The C-C vibrations for hetero aromatic compounds are frequently seen between 1430 and 1650 cm^{-1}. Consequently, the C-C vibrations of 3CBA have been found at 1440, 1396, 1286, 1132 cm^{-1} in the infrared and 1565, 1530, 1450, 1325, 1300, 1275, 1135 cm^{-1} in the Raman with 81-85% PED. It is exceedingly challenging to identify C-N vibrations because of the blending of several bands. The range 1382–1266 cm^{-1} has been classified as the C–N stretching absorption by Socrates[26]. In this study, the C–N stretching mode is assigned at 1264 cm^{-1} in IR and 1250 cm^{-1} in Raman, which are supported by its PED (80%).The C-C and C-N in-plane bending vibrations are found as medium strong band at 786 cm^{-1} in FTIR and veryweak band at 865 cm^{-1}in the FT-Raman spectrum, respectively. The out-of-plane bending vibrations of C-C and C-N have been identified at 375 cm^{-1} and 350 cm^{-1} in the Raman spectrum which are supported by their PED (60%).

C-Cl vibrations

A large range between 760 and 370 cm^{-1} is often produced when a halogen atom is physically linked to a benzene ring, since the C–Cl stretching vibrations tend to pair with ring vibration[27]. The C-Cl stretching vibration of 3CBA is identified at 764 cm^{-1} in the FTIR and 712 cm^{-1} in the FT-Raman spectrum. These wavenumbers exhibit considerable intensity and are in agreement with the theoretical values calculated at 731 cm^{-1} (72% PED). Their substantial coupling with other modes is demonstrated by PED values. The in-plane and out-of-plane C-Cl modes of 3CBA are also listed in Table 3.

Frontier molecular orbitals and DOS spectrum

The highest occupied molecular orbitals (HOMOs) are orbitals that have external electrons and have the ability to transfer electrons to free metal orbitals (FMOs). The lowest unoccupied molecular orbitals (LUMO) are comparable to the initial excited state that can take electrons[28]. To investigate how the solvent influenced the compound's electronic structure, the oscillator strength, wavelength, excitation energies, and significant contributions have been estimated at both diffuse functions (TD-DFT/B3LYP/6-311+G(d,p) and 6-311++G(d,p)) for 3CBA in gas phase, methanol and ethanol. The global reactivity characteristics of 3CBA have been computed at the DFT level using various diffuse functions and solvents, utilizing Koopman's theorem[29] and are shown in (Table 4). The gas phase electron affinity value (A = 1.7692 eV) and ionization potential (I = 7.2090 eV) indicate that the 3CBA molecule will function as a very good donor and acceptor of electrons. The ionization potential and electron affinity for 3CBA are calculated to be I = 7.220 eV and A = 1.7474 eV and I = 7.2198 eV and A = 1.7469 eV, in methanol and ethanol, respectively. A hard molecule has a large energy gap in contrast to a soft molecule's small, low energy gap.It has been determined that 3CBA has the following gas phase hardness (η) and softness (S): 2.7199 eV and 0.1838 eV^{-1}, respectively. In methanol and ethanol, 3CBA has the following chemical

Table 4 — Global reactivity descriptors for 3-chlorobenzamide

Molecular Properties	B3LYP/6-311+G(d,p)			B3LYP/6-311++G(d,p)		
	Gas phase	Methanol	Ethanol	Gas phase	Methanol	Ethanol
HOMO (eV)	-7.2090	-7.220	-7.2204	-7.2090	-7.220	-7.2198
LUMO (eV)	-1.7687	-1.7472	-1.7469	-1.7692	-1.7474	-1.7469
ΔE (E_{HOMO} -E_{LUMO}) (eV)	5.4403	5.4728	5.4735	5.4398	5.4726	5.4729
Ionization potential (I) (eV)	7.2090	7.220	7.2204	7.2090	7.220	7.2198
Electron affinity (A) (eV)	1.7687	1.7472	1.7469	1.7692	1.7474	1.7469
Global hardness(η) (eV)	2.7201	2.7364	2.7367	2.7199	2.7363	2.7364
Global softness (s) (eV^{-1})	0.1838	0.1827	0.1826	0.1838	0.1827	0.1827
Electronegativity (χ) (eV)	4.4888	4.4836	4.4836	4.4891	4.4837	4.4834
Chemical potential (μ) (eV)	-4.4888	-4.4836	-4.4836	-4.4891	-4.4837	-4.4834
Global electrophilicity (ω) (eV)	3.7037	3.6731	3.6728	3.7045	3.6734	3.6708

hardness and softness values: 2.7363 eV and 0.1827 eV^{-1} and 2.7364 eV and 0.1827 eV^{-1}. A molecule's reactivity increases when its electronic chemical potential (μ) drops. The chemical potential (μ) of 3CBA for gas phase, methanol and ethanol is determined to be -4.4891, -4.4837, and -4.4834 eV, respectively. 3CBA is more reactive in ethanol because its chemical potential in ethanol is lower than those of gas phase and methanol. Electronegativity (φ) is defined as the opposite of the chemical potential. The 3CBA molecule is a superior electron acceptor comes from the higher electronegativity (χ) of 4.4891 eV, in gas phase. Using the electrophilicity (ω) scale developed by Domingo *et al.*[30], organic compounds may be categorized as marginal electrophiles ($\omega < 0.8$ eV), moderate electrophiles ($0.8 < \omega < 1.5$ eV), and strong electrophiles ($\omega > 1.5$ eV). The 3CBA's electrophilicity index (ω) is found to be 3.7045, 3.6734 and 3.6708 eV in the gas phase, methanol and ethanol solvents, respectively. These results suggest that the compound is a potent electrophile. Figure 4 depicts a three-dimensional illustration of 3CBA border orbitals. The whole C-C bond possesses the benzene ring, which is the delocalized LUMO of π nature. The electron density transfers from the chlorine atom to the C-C bonds are, however, suggested by the HOMO to LUMO transition since the HOMO is positioned on the chlorine atom.

In the two diffuse functions, the observed HOMO energy for 3CBA is -7.2090 eV in gas phase. The orbital has the potential to act as an electron donor because of its greater energy value. Conversely, the 3CBA has the lowest LUMO energy (-1.7492 eV), suggesting that it will act as the electron acceptor. To reflect the chemical activity of 3CBA, the energy gap is determined to be 5.4398 and 5.4729 eV in the gas phase and ethanol basis sets, respectively. The energy gap widens and the molecule gets more stable when it transitions from the gaseous to the solvent phase. Compared to methanol and ethanol (which are extremely polar), the energy gap between HOMO and LUMO for 3CBA are 5.4726 and 5.4729 eV by 6-311++G(d,p) functional and are smaller than gap in gas phase (5.4398 eV). The molecular orbital contributions of 3CBA are given in (Table 5). The UV-visible plot of 3CBA, as shown in (Fig. 5), shows the anticipated peak in the gas phase at 229.26 nm (H→L+1 contribution of 89.3%), in the methanol at 230.47 nm (H-2→L contributes 73.78%) and ethanol at 230.47 nm (H-2→L contributes 75.3%). Consequently, the unsaturation of 3CBA is brought about by the induction of the $\pi \rightarrow \pi^*$ type transition by the aromatic ring contact.

Similar degenerate energy levels can exist between adjacent orbitals in a border zone. If so, using HOMO and LUMO alone to characterize border orbitals may not be appropriate. Consequently, the total of the beta (β) and alpha (α) electron densities of states is the density of states (DOS), which are generated by utilizing the GaussSum 3.0 program to combine the molecular orbital data with Gaussian curves. The system's border orbitals and energy gap composition are displayed in the density of state plot,DOS in 3CBA is occupied by a total of 80 electrons, comprising both 40α and 40β electrons. Figure 6 illustrates how a molecule's orbital configuration affects the chemical bonds that bind its atoms together.

NBO analysis

Since all orbital features are mathematically selected to incorporate the maximum proportion of the electron density, the natural bond orbital (NBO)

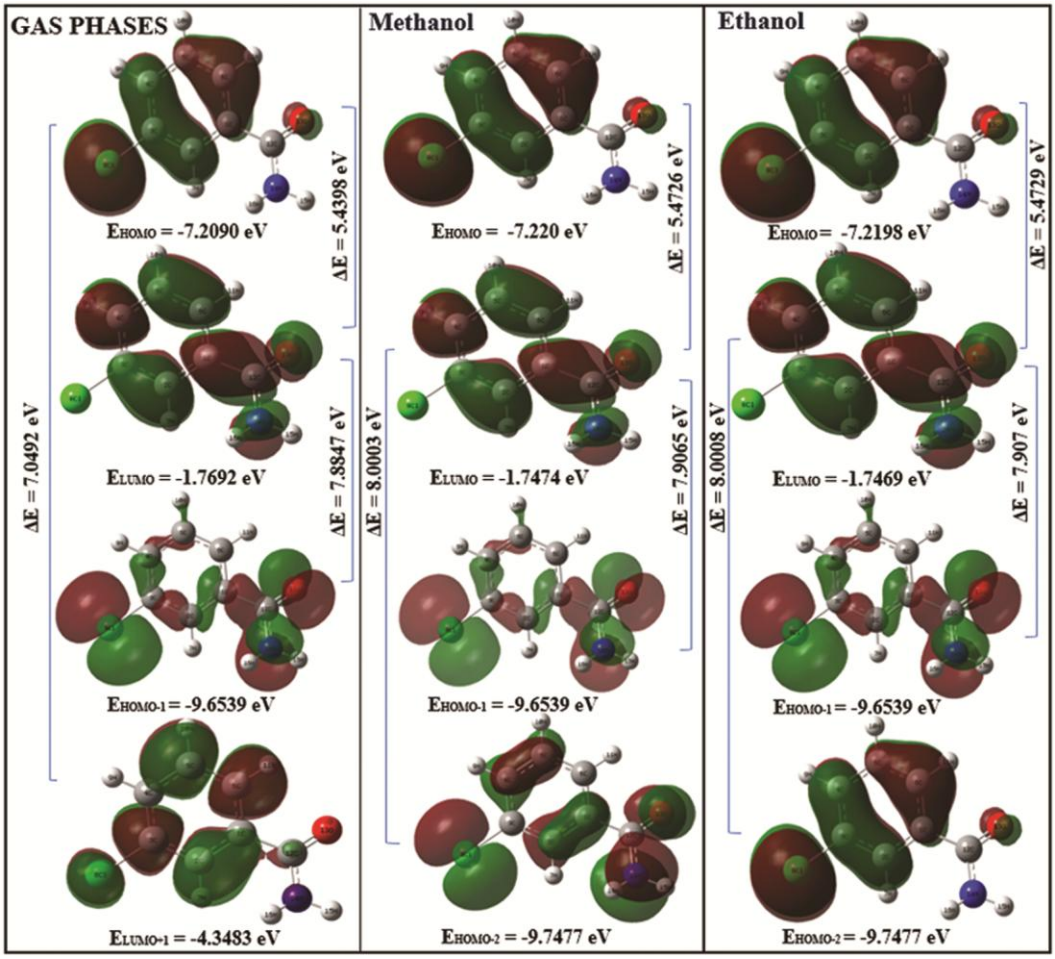

Fig. 4 — HOMO-LUMO plot for 3-chlorobenzamide

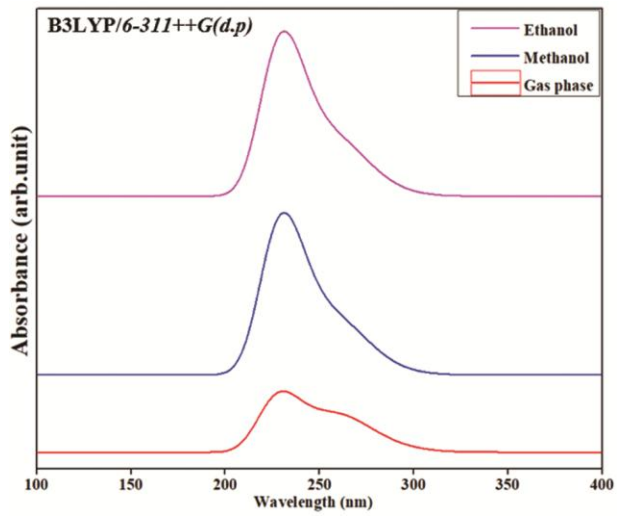

Fig. 5 — UV plot of 3-chlorobenzamide

technique of Reed *et al.*[31] offers the most accurate "natural Lewis structure" depiction. The NBO method's ability to provide information about interactions in both virtual and filled orbital spaces is a helpful feature that may improve the investigation of intra- and intermolecular interactions. The energy of electron transference or hyperconjugative contact has been computed by the application of the second-order perturbation approach. In the NBO study of 3CBA,

Table 5 — Molecular orbital contributions of 3-chlorobenzamide

TD-DFT/ B3LYP/ 6-311++G(d,p)	Gas phase			
Energy (eV)	Oscillator strength	Computed wavelength (nm)	Major contributions	Assignment
5.4079	0.0435	229.26	H→L+1 (89.3%)	π→π*
5.3796	0.1182	Methanol 230.47	H-2→L (73.78%)	π→π*
5.3777	0.1182	Ethanol 230.47	H-2→L (75.3%)	π→π*

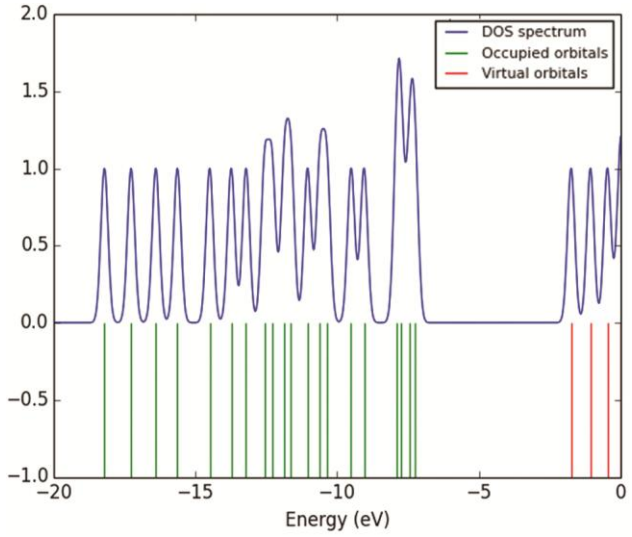

Fig. 6 — DOS Spectrum of 3-chlorobenzamide

the donor-acceptor interactions have been assessed using the second order Fock matrix using the B3LYP technique and the 6-311++G(d,p) basis set. A stabilizing donor-acceptor interaction may be modelled as the delocalization of electron density between formally vacant (antibond or Rydberg) non-Lewis NBO orbitals and occupied Lewis-type (bond or lone pair) NBO orbitals. Table 6 provides an inventory of the corresponding results.

In 3CBA, the orbitals interactions of π(C5-C6)→ π*(C3-C4), π(C5-C6)→ π*(C1-C2), and π(C1-C2)→ π*(C5-C6) have the greatest stabilization energies (23.10, 21.22, and 18.96 kcal mol^{-1}). These interactions cause high electron concentrations in the anti-bonding C-C acceptor orbitals (about 0.38257e, 0.36508e, and 0.29959e). The high interaction between π*(C3-C4) and antibonding orbitals π*(C1-C2) and π*(C5-C6), which have stabilization energies of 237.76 and

Table 6 — Second-order perturbation theory analysis of Fock matrix for 3-chlorobenzamide

Donor(i)	ED (i) (e)	Acceptor (j)	ED (j) (e)	E(2) (kcal/mol)	E (j) −E (i) (arb. units)	F(i,j) (arb. units)
σ(C1-C2)	1.96778	σ*(C1-C6)	0.02090	3.94	1.28	0.063
σ(C1-C2)	1.96778	σ*(C2-C3)	0.02804	3.81	1.27	0.062
σ(C1-C2)	1.96778	σ*(C3-Cl8)	0.03303	4.85	0.85	0.057
π(C1-C2)	1.65791	π*(C3-C4)	0.38257	20.31	0.27	0.067
π(C1-C2)	1.65791	π*(C5-C6)	0.29959	18.96	0.29	0.067
π(C1-C2)	1.65791	π*(C12-O13)	0.27075	15.59	0.31	0.063
σ(C1-C6)	1.97257	σ*(C1-C2)	0.02414	4.04	1.26	0.064
σ(C2-C3)	1.97896	σ*(C1-C2)	0.02414	3.53	1.3	0.06
σ(C2-C3)	1.97896	σ*(C3-C4)	0.02787	3.65	1.29	0.061
σ(C2-H7)	1.97712	σ*(C1-C6)	0.02090	4.09	1.1	0.06
σ(C2-H7)	1.97712	σ*(C3-C4)	0.02787	4.37	1.1	0.062
σ(C3-C4)	1.97984	σ*(C2-C3)	0.02804	3.72	1.29	0.062
π(C3-C4)	1.66932	π*(C1-C2)	0.36508	20.01	0.3	0.069
π(C3-C4)	1.66932	π*(C5-C6)	0.29959	17.17	0.3	0.065
σ(C4-C5)	1.97174	σ*(C3-C4)	0.02787	3.49	1.27	0.059
σ(C4-C5)	1.97174	σ*(C3-Cl8)	0.03303	5.21	0.85	0.059
σ(C4-H9)	1.97853	σ*(C2-C3)	0.02804	4.48	1.09	0.062
σ(C4-H9)	1.97853	σ*(C5-C6)	0.01456	3.47	1.11	0.055
π(C5-C6)	1.64225	π*(C1-C2)	0.36508	21.22	0.28	0.069
π(C5-C6)	1.64225	π*(C3-C4)	0.38257	23.10	0.26	0.07
σ(C5-H10)	1.97957	σ*(C1-C6)	0.02090	3.70	1.09	0.057
σ(C5-H10)	1.97957	σ*(C3-C4)	0.02787	3.44	1.08	0.055
σ(C6-H11)	1.97772	σ*(C1-C2)	0.02414	4.70	1.08	0.064
σ(C6-H11)	1.97772	σ*(C4-C5)	0.01698	3.75	1.08	0.057
π(C12-O13)	1.99357	π*(C1-C2)	0.36508	3.70	0.41	0.038
σ(N14-H15)	1.98971	σ* (C1-C12)	0.07020	3.69	1.08	0.057
σ(N14-H16)	1.98776	σ*(C12-O13)	0.02253	3.49	1.27	0.059
LP (2)Cl8	1.97170	σ*(C2-C3)	0.02804	4.08	0.88	0.053
LP (2)Cl8	1.97170	σ*(C3-C4)	0.02787	4.12	0.88	0.054
LP (3)Cl8	1.92996	π*(C3-C4)	0.38257	12.22	0.33	0.061
LP (2)O13	1.86685	σ*(C1-C12)	0.07020	18.75	0.66	0.101
LP (2)O13	1.86685	σ*(C12-N14)	0.06739	24.86	0.69	0.119
LP (1)N14	1.76470	π*(C12-O13)	0.27075	43.70	0.32	0.107
π*(C1-C2)	0.36508	π*(C12-O13)	0.27075	88.49	0.02	0.07
π*(C3-C4)	0.38257	π*(C1-C2)	0.36508	237.76	0.01	0.081
π*(C3-C4)	0.38257	π*(C5-C6)	0.29959	143.88	0.02	0.083
π*(C12-O13)	0.27075	σ*(C12-O13)	0.02253	4.31	0.54	0.113

143.88 kcal mol^{-1}, indicates a considerable delocalization. Likewise, the amount of the charge transfer from the lone pairs Cl8, O13 and N14 to the antibonding C-C and C-O orbitals are found as 12.22, 18.75 and43.70 kcal mol^{-1}. The strong hyper conjugative interactions between electronegative chlorine, oxygen and nitrogen atoms and the ring structure result in a significant reduction in the lone pair electron density in comparison to other orbitals.

Mullikan charge analysis

In order to apply quantum mechanical calculations to atomic charges that result in dipole moment, molecule polarizability, and electronic characteristics of molecular systems, it is crucial to calculate Mulliken atomic charges[32]. The distribution of positive and negative charges has a major impact on how long the bonds are between the atoms in a molecule. With methanol and ethanol solvations, the charges on the atoms of 3CBA are computed using Mulliken population analysis utilizing the diffuse functions B3LYP/6–311+G(d,p) and B3LYP/6–311++G(d,p). The results are shown in (Table 7). Figure 7 displays the graphic depictions of Mulliken atomic charges for 3CBA. The largest positive charges are found in carbon atoms C1 and C3 in methanol, ethanol and gas phase, which are 0.899325 and 0.778814, 0.850576 and 0.759541, and 0.851542 and 0.760139, respectively, and C2 is extremely negative (-1.27804 in gas phase). This is because the atom C2 is lying between the chlorine and amide groups. The charges on oxygen (O13) and nitrogen (N14) atoms are negative in all solvent phase and all of the hydrogen atoms in 3CBA are found to have

Table 7 — Mulliken atomic charges for 3-chlorobenzamide

Atoms	Atomic Charges (Mulliken)					
	B3LYP/6-311+G(d,p)			B3LYP/6-311++G(d,p)		
	Gas phase	Methanol	Ethanol	Gas phase	Methanol	Ethanol
C1	0.682515	0.659431	0.659852	0.899325	0.850576	0.851542
C2	-1.13152	-1.08596	-1.08713	-1.27804	-1.20992	-1.21153
C3	0.940222	0.938204	0.938464	0.778814	0.759541	0.760139
C4	-0.56063	-0.56901	-0.56879	-0.5634	-0.56671	-0.5666
C5	-0.28179	-0.30788	-0.30751	-0.16518	-0.21645	-0.21563
C6	-0.22211	-0.23909	-0.2386	-0.55656	-0.556	-0.55586
H7	0.144292	0.167614	0.167225	0.168586	0.200774	0.200215
Cl8	0.374567	0.346329	0.346671	0.442234	0.416058	0.416363
H9	0.153097	0.172625	0.172323	0.182769	0.209006	0.208606
H10	0.139913	0.16217	0.161825	0.182509	0.210647	0.210217
H11	0.159535	0.160948	0.160965	0.19151	0.191511	0.191581
C12	-0.19873	-0.1564	-0.1571	-0.15163	-0.10399	-0.10487
O13	-0.3295	-0.41373	-0.41235	-0.31697	-0.40289	-0.40148
N14	-0.39146	-0.4187	-0.41834	-0.36289	-0.39006	-0.3897
H15	0.294714	0.31832	0.318006	0.320867	0.341804	0.341534
H16	0.226869	0.265142	0.264489	0.22804	0.266108	0.265474

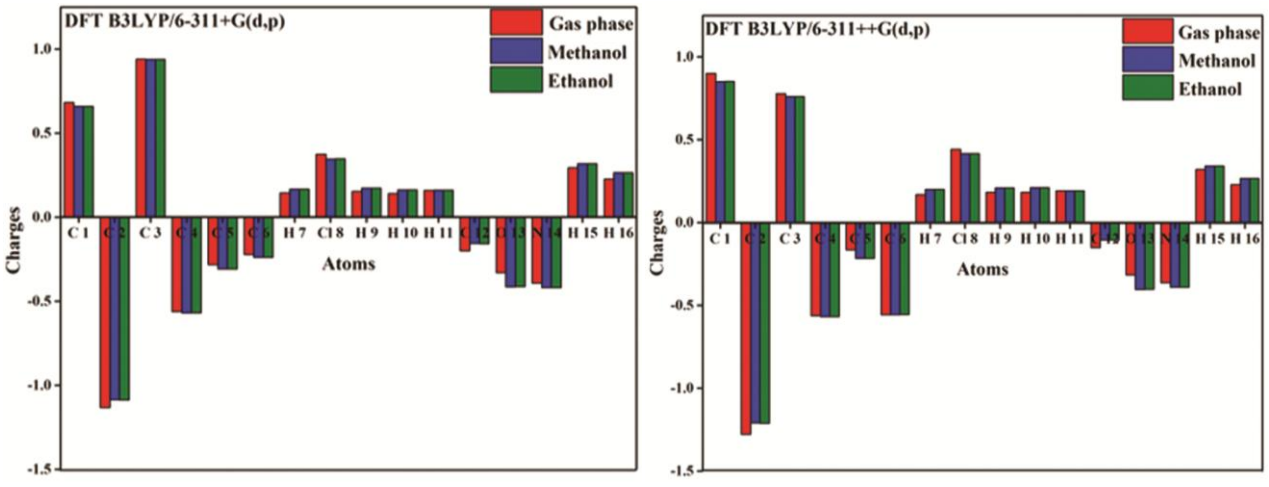

Fig. 7 — Mulliken charges plot for 3-chlorobenzamide

positive charges. Hence, the molecule is very acidic, as shown by the optimistic hydrogen atoms' charges for H7, H9, H10, H11, H15, and H16 (0.168586, 0.182769, 0.182509, 0.19151, 0.32.867, and 0.22804 correspondingly) in 3CBA. Moreover, it is demonstrated that the positive charges of donor atom Cl8 decreases as it moves from the gas phase (0.442234) to the methanol and ethanol (0.416058 and 0.416363). Therefore, raising the solvent's dielectric constant is necessary to make a meaningful change in the 3CBA.

Fukui function

The Fukui function, also known as the frontier function, is utilized to forecast a molecule's reactivity sites and to identify electrophilic and nucleophilic attacks, respectively. The condensed form of the Fukui function[33] for an atom k in a molecule can be defined as,

$$f_k^+ = q_j(N+1) - q_j(N)$$

$$f_k^- = q_j(N) - q_j(N-1)$$

$$f_k^0 = \frac{1}{2}[q_j(N+1) - q_j(N-1)]$$

These are the free radical f_k^0, electrophilic f_k^-, and nucleophilic f_k^+ functions of 3CBA. Here, the symbol q_j stands for the atomic charge at the j^{th} site in the cationic (N-1) and anionic (N+1) chemical species. *Morell et al.*[34], have recently presented a dual descriptor, which is defined as the difference between the nucleophilic and electrophilic functions as given by,

$$\Delta f(r) = f_k^+ - f_k^-$$

The aforementioned equations, which assess reactivity at atomic resolution, have been used to describe the Fukui function and ascertain the pin point distribution of the atomic sites on 3CBA. In this instance, the Fukui function of 3CBA at the two diffuse functions B3LYP/6-311++G(d,p) and B3LYP/6-311+G(d,p) has been determined via Mulliken population analysis. The dual descriptor distinguishes between nucleophilic and electrophilic attacks at a given site are based on their sign. In this study, the nucleophilic sites for 3CBA include C1, C2, C3, C5, Cl8, O13 and N14, which meet the criteria of the dual descriptor, according to the positive values by B3LYP/6-311++G(d,p) as displayed in (Table 8). Conversely, the electrophilic sites are located at atoms C4, C6, H7, H9, H10, H11, C12, H15 and H16, which have negative values. Depending on its local behavior, the molecule 3CBA responds to both nucleophilic and electrophilic assaults during the process.

Molecular electrostatic potentials (MEP)

By using its various colour codes, MEP can assist in illuminating the chemical bonding reaction's receptive regions[35]. The MEP increases our

Table 8 — Fukui functions for 3-chlorobenzamide

B3LYP/6-311+G(d,p)							B3LYP/6-311++G(d,p)						
Mulliken Charges			Fukui functions				Mulliken Charges			Fukui functions			
q(N+1)	q(N)	q(N-1)	f_k^+	f_k^-	f_k^0	$\Delta f(r)$	q(N+1)	q(N)	q(N-1)	f_k^+	f_k^-	f_k^0	$\Delta f(r)$
0.712597	0.682515	0.717115	0.030082	-0.0346	-0.00226	0.064682	1.16327	0.899325	0.950509	0.263945	-0.05118	0.106381	0.315129
-1.16639	-1.13152	-1.05955	-0.03487	-0.07197	-0.05342	0.037096	-1.21123	-1.27804	-1.24294	0.066809	-0.0351	0.015854	0.10191
0.993652	0.940222	0.878886	0.05343	0.061336	0.057383	-0.00791	1.050368	0.778814	0.726827	0.271554	0.051987	0.161771	0.219567
-0.76059	-0.56063	-0.47537	-0.19996	-0.08526	-0.14261	-0.1147	-0.90004	-0.5634	-0.49589	-0.33664	-0.06751	-0.20208	-0.26913
-0.297	-0.28179	-0.24134	-0.01522	-0.04045	-0.02783	0.025235	0.029676	-0.16518	-0.12281	0.194851	-0.04237	0.076243	0.237216
-0.39631	-0.22211	-0.17049	-0.1742	-0.05161	-0.11291	-0.12259	-1.0443	-0.55656	-0.53724	-0.48774	-0.01932	-0.25353	-0.46842
0.098233	0.144292	0.188597	-0.04606	-0.04431	-0.04518	-0.00175	0.113396	0.168586	0.221936	-0.05519	-0.05335	-0.05427	-0.00184
0.237503	0.374567	0.648844	-0.13706	-0.27428	-0.20567	0.137213	0.345314	0.442234	0.716501	-0.09692	-0.27427	-0.18559	0.177347
0.094281	0.153097	0.209542	-0.05882	-0.05645	-0.05763	-0.00237	0.101112	0.182769	0.250495	-0.08166	-0.06773	-0.07469	-0.01393
0.080467	0.139913	0.198323	-0.05945	-0.05841	-0.05893	-0.00104	0.111091	0.182509	0.253281	-0.07142	-0.07077	-0.0711	-0.00065
0.113874	0.159535	0.212713	-0.04566	-0.05318	-0.04942	0.007517	0.123505	0.19151	0.250353	-0.06801	-0.05884	-0.06342	-0.00916
-0.27525	-0.19873	-0.18816	-0.07652	-0.01057	-0.04355	-0.06595	-0.2034	-0.15163	-0.11859	-0.05177	-0.03304	-0.0424	-0.01873
-0.45909	-0.3295	-0.15755	-0.12959	-0.17195	-0.15077	0.04236	-0.43139	-0.31697	-0.14596	-0.11442	-0.17102	-0.14272	0.056596
-0.42153	-0.39146	-0.35343	-0.03007	-0.03803	-0.03405	0.007963	-0.32263	-0.36289	-0.32337	0.040252	-0.03952	0.000367	0.07977
0.245453	0.294714	0.335366	-0.04926	-0.04065	-0.04496	-0.00861	0.143958	0.320867	0.359658	-0.17691	-0.03879	-0.10785	-0.13812
0.200107	0.226869	0.256483	-0.02676	-0.02961	-0.02819	0.002852	-0.0687	0.22804	0.257227	-0.29674	-0.02919	-0.16296	-0.26755

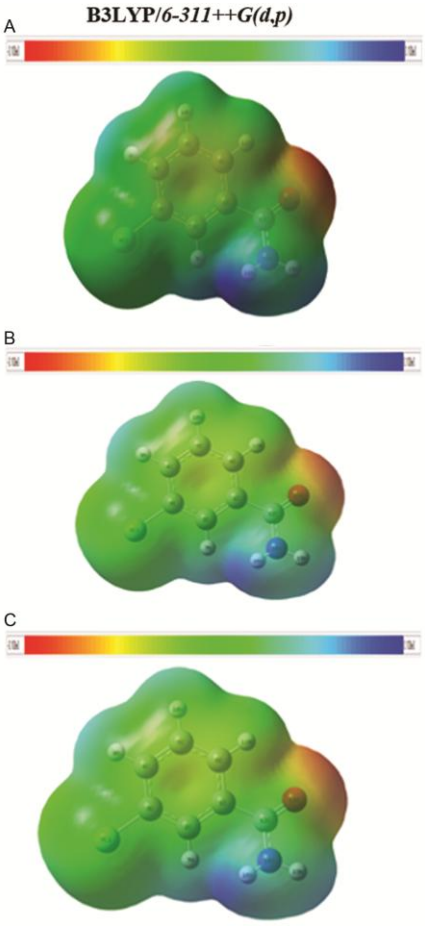

Fig. 8 — MEP plot of 3-chlorobenzamide in (A) Gas phase (B) Methanol; and (C) Ethanol

understanding of electrophilic reactions, molecular reactivity, substituent effects, and inter-intramolecular interactions by establishing connections with the chemically active regions of molecules[36]. In this study, the MEP surfaces of 3CBA in the gas phase, methanol and ethanol have been computed at B3LYP/6-311++G(d,p) and the MEP contours of 3CBA are shown in (Fig. 8). The red, yellow, blue, and green colours have progressively stronger electrostatic potentials. The study's most promising red section clearly demonstrates the oxygen atom's (O13) electrophilic nature. All hydrogens have nucleophilic patches clustered together; the most abundant is the hydrogen (H16) coupled to nitrogen atom (N14). The ring system of 3CBA is surrounded by the neutral electrostatic potentials (green). Furthermore, the green, blue, and red colour on the carbon, hydrogen and oxygen atoms, respectively, becomes darker when it moves from methanol and ethanol to gas phase; in other words, the intensity of colour changes from gas phase > methanol > ethanol.

Nuclear magnetic resonance (NMR) analysis

One of the most popular methods for determining isotropic nuclear magnetic shielding of a molecule is the *Gauge independent atomic orbital* (GIAO) technique[37]. The ^{13}C and ^{1}H NMR chemical shift calculations of 3CBA have been performed in gas phase, methanol and ethanol by GIAO method, utilizing diffuse functions B3LYP/6-311+G(d,p) and 6-311++G(d,p). The results are displayed in Table 9 and the ^{13}C and ^{1}H NMR spectra of 3CBA are shown in (Fig. 9). There is a good agreement between the computed and experimental chemical shifts[38]. An organic molecule's normal ^{13}C NMR chemical shift range is typically >100 ppm. In the current investigation, the ^{13}C NMR chemical shifts for 3CBA are >100 ppm, as would be predicted.

The greatest anticipated ^{13}C NMR shift for C12 is caused by the least effective shielding from nitrogen (N14) and oxygen (O13) atoms. The computed shifts for C12 are found to be 169.931, 172.987 and 172.638 ppm in the gas phase, methanol and ethanol, respectively, and it fits the observed shift rather well as shown in (Fig. 9). The increased shielding effect of the neighboring chlorine nuclei (Cl8) causes a little chemical shift in the carbon atom C2 associated with the ring system at 130.199, 131.696 and 131.665 ppm in gas phase, methanol and ethanol, respectively. When hydrogen atoms are put near to or directly connected to an atom that accepts electrons, their resonance and shielding are diminished, resulting in a higher wavenumber. In 3CBA, the minimum chemical shifts are obtained for H15 and H16 as 4.5715 and 5.0519 ppm, in gas phase, since they are connected tightly to the nitrogen atom (N14).

Molecular docking study

Molecular docking is a computer programmer used in pharmacological drug development that looks at protein and ligand binding sites[39,40]. It is used to investigate how target proteins' amino acid residues and hydrogen bonds interact with the ligand molecule. Based on prior research, we have chosen ovarian and breast cancer proteins[41,42], which include human Matrix metalloproteinase-2 (MMP-2) receptors (PDB ID: 7XJO and PDB ID: 7XGJ), human progesterone (PDB ID: 4OAR) and allosteric inhibitor (PDB ID: 5KCV) receptors for 3CBA docking computations[43]. In comparison to standard medications for ovarian and breast cancer, the X-ray crystallographic structures of carboplatin and anastrozole have been

Table 9 — ^{13}C and ^{1}H NMR chemical and shifts for 3-chlorobenzamide

Atoms	B3LYP/*6-311+G(d,p)*			B3LYP/*6-311++G(d,p)*		
	Gas phase Calculated Shift (ppm)	Methanol Calculated Shift (ppm)	Ethanol Calculated Shift (ppm)	Gas phase Calculated Shift (ppm)	Methanol Calculated Shift (ppm)	Ethanol Calculated Shift (ppm)
C1	141.196	140.871	140.877	141.276	140.954	140.96
C2	130.059	131.554	131.524	130.199	131.696	131.665
C3	148.286	147.83	147.83	148.285	147.831	147.832
C4	136.175	137.446	137.425	136.228	137.487	137.466
C5	134.161	134.831	134.823	134.298	134.947	134.939
C6	133.85	132.379	132.399	133.18	132.476	132.497
H7	7.5936	7.8597	7.8547	7.6067	7.8733	7.8684
H9	7.4935	7.7039	7.7005	7.4863	7.6951	7.6917
H10	7.4486	7.66	7.6568	7.4635	7.6718	7.6686
H11	8.1779	8.1219	8.1235	8.1772	8.121	8.1227
C12	169.846	172.9	172.851	169.931	172.987	172.638
H15	4.5725	5.0262	5.0196	4.5715	5.0244	5.0178
H16	5.0505	5.7101	5.6982	5.0519	5.7109	5.699

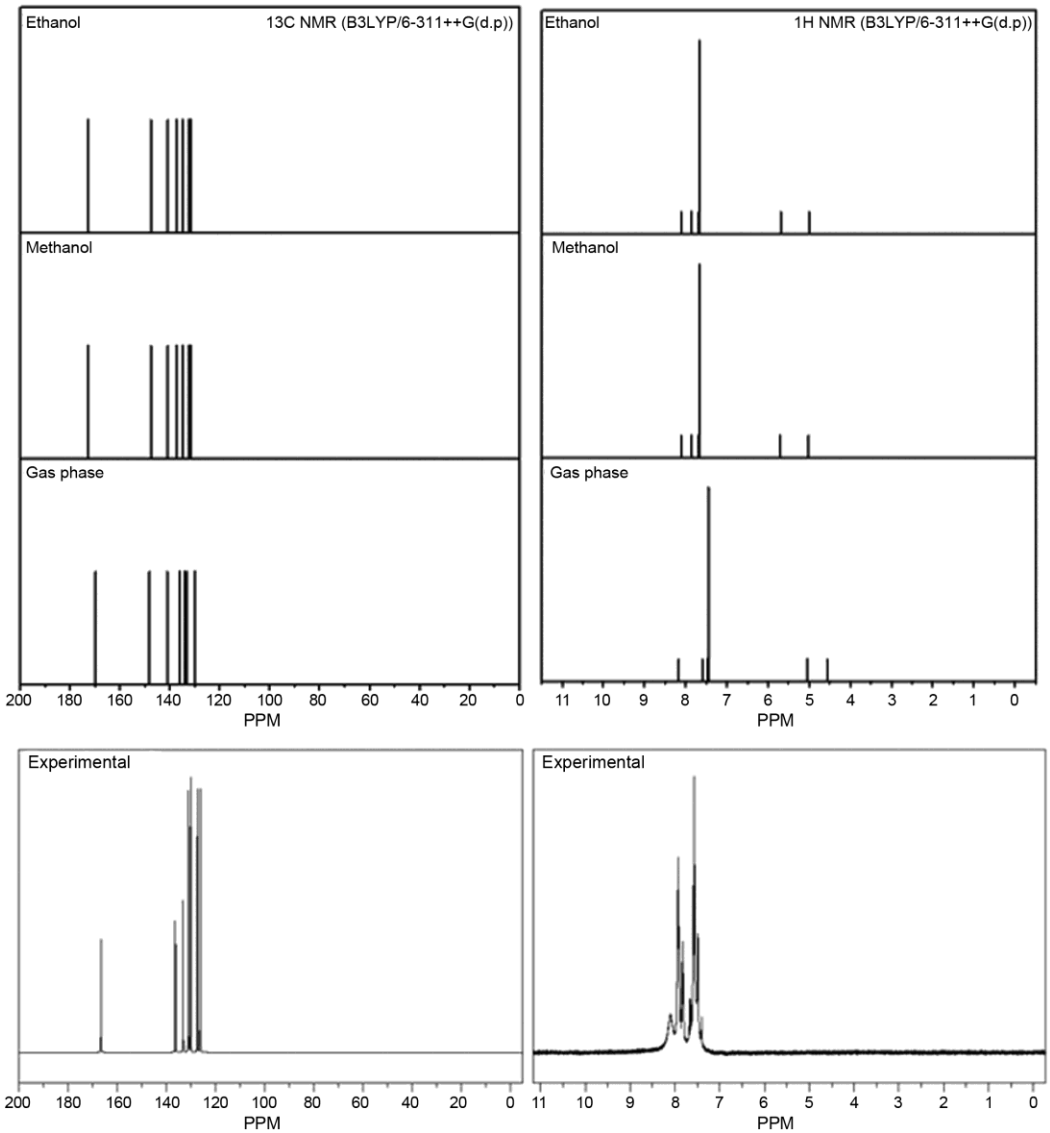

Fig. 9 — ^{13}C and ^{1}H NMR plot of 3-chlorobenzamide

Table 10 — Comparison of binding affinity of 3-chlorobenzamide with 7XJO, 7XGJ, 4OAR and 5KCV along with standard drugs Carboplatin and Anastrozole

S. No.	Type of cancer	Standard cancer drugs	Bindingaffinity (kcal/mol)	Interacted Residues	H-bonding involved between ligand and protein	Protein	Bindingaffinity (kcal/mol)	Interacted Residues	H-bonding involved between ligand and protein
1	Anti-ovarian cancer activity	Carboplatin	-5.1	LEU A: 138, ALA A: 137, THR A: 144, TYR A: 143, LEU A: 117	LEU A: 138, ALA A: 137, THR A: 144	7XJO	-6.5	ALA A :140, LEU A:138, ALA A:137, HIS A: 121, TYR A: 143	ALA A :140, LEU A:138, ALA A:137
2						7XGJ	-6.4	LEU A: 138, ALA A:137, THR A:144, LEU A:83, HIS A:121, VAV A:118, TYR A:143	LEU A: 138, ALA A:137, THR A:144
3	Anti-breast cancer activity	Anastrozole	-5.9	LEU A; 687, GLU A: 843	GLU A: 843	4OAR	-6.0	LEU A: 758, MET A:759, ARG A:766, PRO A:696, LYS A:822, TRP A:732, VAL A:729	LEU A: 758, MET A:759, ARG A:766
4						5KCV	-5.7	TRP A:413, TYR A:417	TRP A:413

chosen. As seen from (Table 10), the strongest interactions of 3CBA are found with the 7XJO and 7XGJ proteins, where it delivered the greatest binding affinity. With a binding affinity of -6.5 kcal mol^{-1}, these linkages provide the most feasible interaction between protein 7XJO and 3CBA when compared to typical medications (Carboplatin) with a binding affinity of -5.1 kcal mol^{-1}.

According to our findings, 3CBA interacts with the 7XJO receptor via three typical hydrogen bonds as shown in (Fig. 10A), with the distances between the ALA A:140, LEU A:138, and ALA A:137 residues being 2.05, 2.94, and 2.42 Å, respectively. More research revealed that 3CBA interacts with 7XGJ receptor more firmly by three hydrogen bonds through LEU A:138, ALA A:137, and THR A:144 residues separated by bond distances of 2.27, 2.25, and 2.24 Å, respectively. The binding affinity of the 7XGJ protein and 3CBA has been determined to be -6.4 kcal mol^{-1}. In 3CBA, the residues LEU A:758 (2.30 Å), MET A:759 (2.64 Å), ARG A:766 (2.28 Å), and TRP A:413 (2.57 Å) each have one hydrogen bond interaction with each of the receptors 4OAR and 5KCV, respectively, as shown in (Fig. 10B). Furthermore, the ligand 3CBA has a good binding affinity for the proteins 4OAR and 5KCV (-6.0 and -5.7 kcal mol^{-1}, respectively). The binding affinity of 4OAR receptor is more than that of the conventional drug Anastrozole, which has binding affinity of -5.9 kcal mol^{-1}. As a result, the 3CBA ligand interacts best with ovarian and breast cancer proteins, and it may be able to inhibit their activity.

ADMET prediction

One of the primary requirements for turning a chemical into a medicine is the evaluation of its Absorption, Distribution, Metabolism, and Excretion (ADMET) characteristics[44,45]. Previously, many drug candidates were unable to fulfill clinical trial requirements; hence, computer-based prediction is crucial in the early phases of prediction. Before medicine is excreted from the body via urine and faeces, the ADMET profile has a direct impact on physiochemical properties such as hydrophobicity, lipophilicity, gastrointestinal environment, and blood-brain barrier integrity. ADMET properties of 3CBA were assessed using the publically accessible web-based programme (http://biosig.unimelb.edu.au/pkcsm/prediction). Table 11 shows a number of ADMET characteristics of 3CBA.

Based on ADMET characteristics collected from the ADMET-SAR service, the chemical 3CBA has a higher human intestine absorption score (92.799%). The LD_{50} is essential for predicting the symptoms of

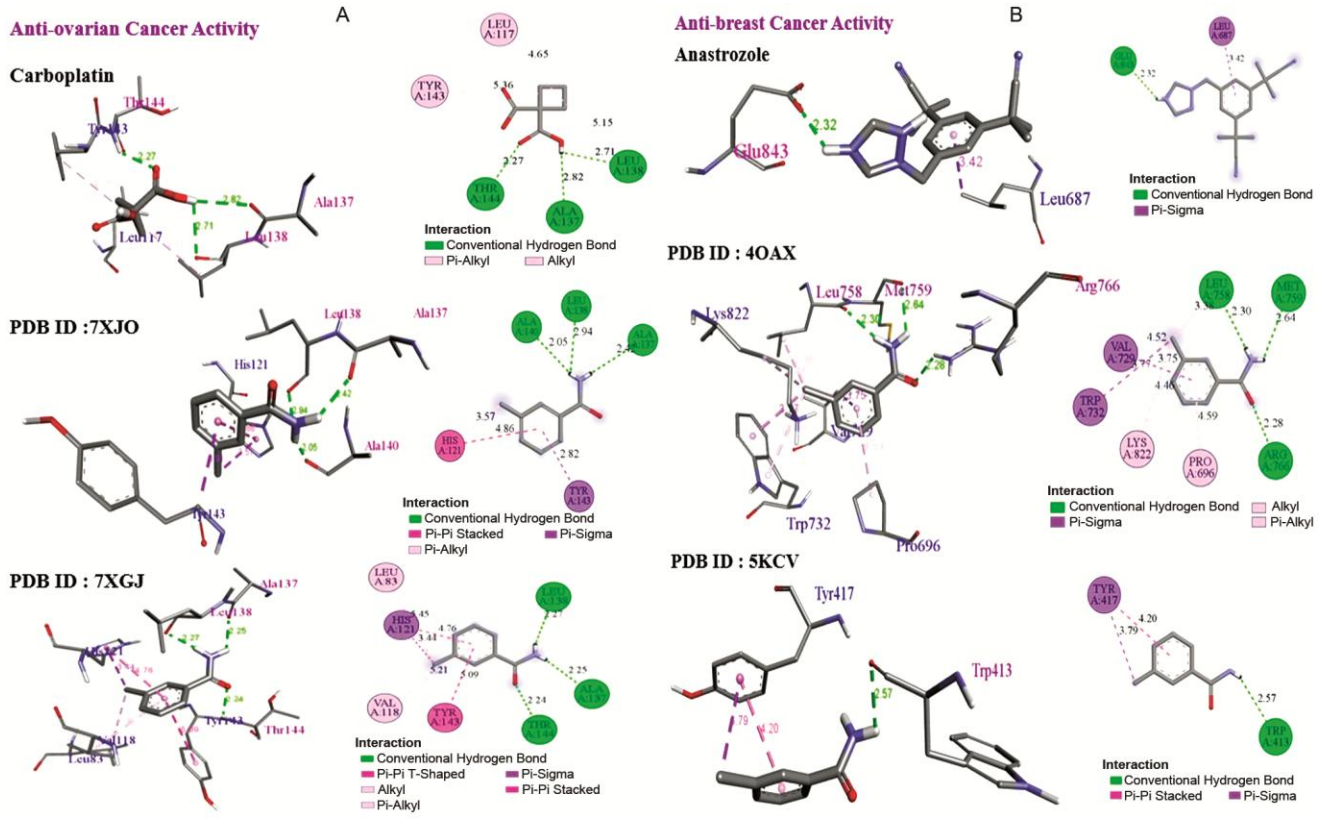

Fig. 10 — (A) Binding interaction and anti-ovarian cancer activity of 3-chlorobenzamide; and (B) Binding interaction and anti-breast cancer activity of 3-chlorobenzamide

Table 11 — ADMET profile of 3-chlorobenzamide

ADMET prediction	Value	ADMET prediction	Value
CaCo-2 permeability (log Papp in 10^{-6} cm/s)	1.241	P-glycoprotein substrate	No
Intestinal absorption (human) (%)	92.799	P-glycoprotein I inhibitor	No
Skin Permeability (log Kp)	-2.446	P-glycoprotein II inhibitor	No
VDss (human) (log L/kg)	-0.054	Total Clearance (log ml/min/kg)	0.011
Fraction unbound (human) (Fu)	0.465	Renal OCT2 substrate	No
BBB permeability (log BB)	-0.26	AMES toxicity test	No
CNS permeability (log PS)	-2.044	Max. tolerated dose (human) (log mg/kg/day)	1.026
CYP2D6 substrate	No	hERG I inhibitor	No
CYP3A4 substrate	No	hERG II inhibitor	No
CYP1A2 inhibitor	Yes	Oral Rat Acute Toxicity (LD50) (mol/kg)	2.24
CYP2C19 inhibitor	No	Oral Rat Chronic Toxicity (LOAEL) (log mg/kg_bw/day)	1.536
CYP2C9 inhibitor	No	Hepatotoxicity	No
CYP2D6 inhibitor	No	Skin Sensitisation	Yes
CYP3A4 inhibitor	No	T.Pyriformistoxicity (log ug/L)	0.279
Carcinogenicity	No	Minnow toxicity (log mM)	1.841

poisoning that result from an acute overdose in humans. The LD50 of 3CBA is found to be 2.24 mol/kg, and the molecule's blood-brain barrier (BBB) penetration rate is extraordinary (-0.26). Based on these findings, 3CBA revealed significant plasma protein binding, excellent blood brain barrier bridging, and the possibility of intestinal absorption in humans. Consequently, the results of this new study will help in the creation of anti-cancer medications.

Conclusion

The 6-311+G(d,p) and 6-311++G(d,p) diffuse functions are used to calculate the optimized geometries and normal modes of 3-chlorobenzamide using the DFT/B3LYP technique and almost all the results are equal in both functions. There is a strong correlation between the computed and observed frequencies. In 3CBA, the HOMO is positioned on the chlorine atom, the HOMO to LUMO transition

suggests that the electron density passes from the chlorine atom to the C-C bonds. By looking at the gas phase, methanol, and ethanol, the molecule's energy gap is found to be 5.4398, 5.4726, and 5.4729 eV. Its chemical and biological properties have been identified, along with global reactivity descriptors and DOS spectra. The ionization potential (I = 7.2090 eV) and gas phase electron affinity value (A = 1.7692 eV) suggest that the 3CBA molecule will be an excellent electron giver and acceptor. The electronic transition fell into the same range (230.47 nm) in both methanol and ethanol solvents. The antibonding C-C and C-O orbitals get a charge transfer of 12.22, 18.75, and 43.70 kcal mol^{-1} from the lone pairs Cl8, O13, and N14. Fukui functions and Mulliken charge studies determined that the ring and substitution atoms (chlorine, oxygen and nitrogen) are the most likely sites for electrophilic and nucleophilic assaults. Also, the electrophilic (O13) and nucleophilic (H16) reactivity sites are represented by the MEP results. The molecule's proton and carbon NMR shifts have been computed and compared to the findings of the experiment. The molecular docking analysis showed that the 3CBA has the highest binding affinity (-6.5 kcal mol^{-1}) with the human Matrix metalloproteinase-2 (MMP-2) receptor (PDB ID: 7XJO), with which it interacts most. 7XJO's docking exhibited more hydrogen bonding connections than 7XGJ, 4OAR, and 5KCV proteins. Additionally, ADMET testing show that 3CBA will successfully treat ovarian and breast cancers while minimizing the side effects of conventional interventions.

Acknowledgement

The authors would like to thank Kalasalingam Academy of Research and Education's International Research Centre (IRC) for providing funding assistance for the creation of the computational research centre.

Conflict of interest

All authors declare no conflict of interest.

References

1 Dwivedi A & Kumar A, Molecular docking and comparative vibrational spectroscopic analysis, HOMO-LUMO, polarizabilities, and hyperpolarizabilities of N-(4-Bromophenyl)-4-Nitrobenzamide by different DFT (B3LYP, B3PW91, and MPW1PW91) methods. *Polycycl Aromat Compd*, 41 (2019) 387.

2 Krishnakumar V, Murugeswari K & Surumbarkuzhali N, Molecular structure, intramolecular hydrogen bonding and vibrational spectral investigation of 2-fluorobenzamide – A DFT approach. *Spectrochim Acta A Mol Biomol Spectrosc*, 114 (2013**)** 410.

3 Lalitha K, Karnan M, Anuradha M & Karunanidhi M, Vibrational spectroscopic studies, quantum chemical analysis, drug likeness, molecular docking and ADMET scoring function on N,N-dimethylbenzamide. *Stoch Anal Appl*, 26 (2022) 412.

4 Nuta DC, Chifiriuc MC, Draghici C, Limban C, Missir AV & Morusciag L, Synthesis, characterization and antimicrobial activity evaluation of new agents from benzamides class. *Farmacia*, 61 (2013) 966.

5 Kothari R, Agrawal A & Rai S, Synthesis, characterization, molecular docking and antibacterial activities of Bis-[(E)-3{2-(1-4-chlorophenyl) ethylidiene}hydrazinyl]-N-(4-methylphenyl)- 3-oxopropanamide Zinc (II) complex. *Indian J Biochem Biophys*, 59 (2022) 50.

6 Al-Otaibi JS, Mary YS, Mary YS & Thirunavukkarasu M, Conformational, reactivity analysis, wave function-based properties, molecular docking and simulations of a benzamide derivative with potential antitumor activity-DFT and MD simulations. *Polycycl Aromat Compd*, 43 (2023)2015.

7 Warude BJ, Wagh SN & Chatpalliwar VA, Design, docking, MD simulation and in-silco ADMET prediction studies of novel indole based benzamide stargeting estrogen receptor alfa positive for effective breast cancer therapy. *Pharmacia*, 70 (2023) 307.

8 Al-Salim YM & Al-Asadi RH, Synthesis, anti-breast cancer activity, and molecular docking studies of thiourea benzamide derivatives and their complexes with copper ion. *J Nat Prod Res*, 7 (2023) 3158.

9 Jomaa I, Issaoui N, Roisnel T & Marouani H, Insight into non-covalent interactions in a tetrachlorocadmate salt with promising NLO properties: Experimental and computational analysis. *J Mol Struct*, 1242 (2021)130730.

10 Mishra A, Sharma D &Tiwari SN, DFT and molecular docking studies of an antiviral drug: Molnupiravir. *Indian J Biochem Biophys*, 61 (2023) 810.

11 Becke AD, Density-functional thermochemistry. III. The role of exact exchange. *J Chem Phys*, 98 (1993) 5648.

12 Gariganti N, Loke SK, Pagadala E, Chinta P, Poola B, Chetti P, Bansal A, Ramachandran B, Srinivasadesikan V & Kottalanka RK, Design, Synthesis, anticancer activity of new amide derivatives derived from 1,2,3-triazole-benzofuran hybrids: an insights from molecular docking, molecular dynamics simulation and DFT studies. *J Mol Struct*, 1273 (2023) 134250.

13 Ganjipour G, Heshmati M, Hashemi M &Entezari M, Administration of Curcumin, Betanin, and CoQ10 combined with nickel oxide, iron superoxide nanoparticles show preventive effects in breast cancer: Effect on apoptosis pathway and MiR-455 expression. *Indian J Biochem Biophys*, 60 (2023) 790.

14 Latha V, Gomathi V, Rajeshkanna A & Ram SH, Generating a potent inhibitor against MCF7 breast cancer cell through artificial intelligence based virtual screening and molecular docking studies. *Indian J Biochem Biophys*, 60 (2023) 844.

15 Frisch MJ, Trucks GW, Schlegel HB, Scuseria GE, Robb MA, Cheeseman JR, Scalmani G, Barone V, Petersson GA, Nakatsuji H, Li X, Caricato M, Marenich A,

Bloino J, Janesko BG, Gomperts R, Mennucci B, Hratchian HP, Ortiz JV, Izmaylov AF, Sonnenberg JL, Williams-Young D, Ding F, Lipparini F, Egidi F, Goings J, Peng B, Petrone A, Henderson T, Ranasinghe D, Zakrzewski VG, Gao J, Rega N, Zheng G, Liang W, Hada M, Ehara M, Toyota K, Fukuda R, Hasegawa J, Ishida M, Nakajima T, Honda Y, Kitao O, Nakai H, Vreven T, Throssell K, Jr. Montgomery JA, Peralta JE, Ogliaro F, Bearpark M, Heyd JJ, Brothers E, Kudin KN, Staroverov VN, Keith T, Kobayashi R, Normand J, Raghavachari K, Rendell A, Burant JC, Iyengar SS, Tomasi J, Cossi M, Millam JM, Klene M, Adamo C, Cammi R, Ochterski J W, Martin RL, Morokuma K, Farkas O, Foresman JB & Fox DJ, Gaussian 09, Revision A.02, GaussianInc, Wallingford CT, (2009).

16 Dennington R, Keith T & Millam J, GaussView, Version 5, Semichem Inc., Shawnee Mission KS, (2009).

17 Jamroz MH, Vibrational energy distribution analysis: VEDA 4 Program, Warsaw, Poland, (2004).

18 Barfield M & Fagerness P, Density functional theory/GIAO studies of the 13C, 15N, and 1H NMR chemical shifts in aminopyrimidines and aminobenzenes: Relationships to electron densities and amine group orientations. *J Am Chem Soc*, 119 (1997) 8699.

19 O'boyle NM, Tenderholt AL & Langner KM, Cclib: A library for package-independent computational chemistry algorithms. *J Comput Chem*, 29 (2007) 839.

20 Trott O & Olson AJ, AutoDock Vina: improving the speed and accuracy of docking with a new scoring function, efficient optimization, and multithreading. *J Comput Chem*, 31 (2009) 455.

21 Seeliger D & de Groot BL,Ligand docking and binding site analysis with PyMOL and Autodock/Vina. *J Comput Aided Mol Des*, 24 (2010) 417.

22 Mohan UP, Kunjiappan S, Pichiah PBT & Arunachalam S, Adriamycin inhibits glycolysis through downregulation of key enzymes in *saccharomyces cerevisiae*. *3 Biotech*, 11 (2021) 15.

23 Srivastava R, Gupta SK, Naaz F, Sen Gupta PS, Yadav M, Singh VK, Singh A, Rana MK, Gupta SK, Schols D & Singh RK, Alkylated benzimidazoles: design, synthesis, docking, DFT analysis, ADMET property, molecular dynamics and activity against HIV and YFV. *Comput Biol Chem*, 89 (2020) 107400.

24 Rauf MK, Bolte M & Badshah A, N-(Benzothia-zol-2-yl)-3-chloro-benzamide. *Acta Crystallogr Sect E Struct Rep Online*, 65 (2009) o1245.

25 Merrick JP, Moran D & Radom L, An evaluation of harmonic vibrational frequency scale factors. *J Phys Chem A*, 111 (2007) 11683.

26 Socrates G, Infrared and Raman Characteristic Group Frequencies. *John Wiley & Sons*, New York, (2001).

27 Viji A, Vijayakumar R, Balachandran V, Vanasundari K & Janaki M, Molecular docking and computational studies investigation on a bioactive anti-cancer drug: Thiazole derivatives. *Indian J Chem Tech*, 29 (2022) 616.

28 Jeyavijayan S, Molecular structure, spectroscopic (FTIR, FT-Raman, ^{13}C and ^{1}H NMR, UV), polarizability and first-order hyperpolarizability, HOMO–LUMO analysis of 2,4-difluoroacetophenone. *Spectrochim Acta A Mol Biomol Spectrosc*, 136 (2015) 553.

29 YossaKamsi RA, Ejuh GW, Tadjouteu AY, Njeumen CA, Tchoffo F & Ndjaka JMB, Computational study of reactivity and solubility of Rubescin D and E molecules in gas phase and in solvent media using Hartree-Fock and DFT methods. *Chin J Phys*, 60 (2019) 1.

30 Domingo LR, Aurell MJ, Perez P & Contreras R, Quantitative characterization of the global electrophilicity power of common diene/dienophile pairs in Diels–Alder reactions. *Tetrahedron*, 58 (2002) 4417.

31 Reed AE, Curtiss LA, &Weinhold F, Intermolecular interactions from a natural bond orbital, donor-acceptor viewpoint. *Chem Rev*, 88 (1988) 899.

32 Parr RG & Yang W, Quantitative CIDNP evidence for the SH2 reaction of alkyl radicals with grignard reagents. Implication to the iron catalyzed Kharasch reaction. *J Am Chem Soc*, 106 (1984) 4048.

33 Ayers PW & Parr RG, Variational principles for describing chemical reactions: the Fukui function and chemical hardness revisited. *J Am Chem Soc*, 122 (2000) 2010.

34 Morell C, Grand A & Toro-Labbé A, New dual descriptor for chemical reactivity. *J PhysChem A*, 109 (2004) 205.

35 Erdogan T, Computational evaluation of 2-arylbenzofurans for their potential use against SARS-CoV-2: A DFT, molecular docking, molecular dynamics simulation study. *Indian J Biochem Biophys*, 59 (2022) 59.

36 Ourhzif EM, Ketatni EM, Akssira M, Troin Y & Khouili M, Crystal structure, Hirshfeld surface analysis and DFT studies of euphorbioside monohydrate a major bisnorsesquiterpene isolated from *euphorbia resinifera* latex. *J Mol Struct*, 1241 (2021) 130511.

37 Parimala K & Balachandran V, Vibrational spectroscopic (FTIR and FT Raman) studies, first order hyperpolarizabilities and HOMO, LUMO analysis of p-toluenesulfonyl isocyanate using *ab initio* HF and DFT methods. *Spectrochim Acta A Mol Biomol Spectrosc*, 81 (2011) 711.

38 Yang FL, Zhu X, Rao DK, Cao XN, Li K, Xu Y, Hao XQ & Song MP, Highly efficient synthesis of primary amides via aldoximes rearrangement in water under air atmosphere catalyzed by an ionic ruthenium pincer complex. *RSC Adv*, 6 (2016) 37093.

39 Cakmak S & Erdogan T, Some bis (3-(4-nitrophenyl) acrylamide derivatives: Synthesis, characterization, DFT, antioxidant, antimicrobial properties, molecular docking and molecular dynamics simulation studies. *Indian J Biochem Biophys*, 60 (2023) 209.

40 Rani UK, Sharma GVM, Saxena S, Guruprasad L & Padmavathi DA, Synthesis, DFT and molecular docking study of novel bis 1,2,3-triazole derivatives of 2-hydroxyquinoline-4-carboxylate as antimicrobial agents. *Indian J Biochem Biophys*, 60 (2023) 729.

41 Priyadharshini S, Swaroop AK, Jubie S, Jawahar N & Divecha V, Molecular docking and cytotoxicity interactions of naringenin and its nano structured lipid carriers in ERα positive breast cancer. *Indian J Biochem Biophys*, 60 (2023) 141.

42 Raja G, Venkatesh G, Al-Otaibi JS, Vennila P, Mary YS & Sixto-López Y, Synthesis, characterization, molecular docking and molecular dynamics simulations of benzamide

derivatives as potential anti-ovarian cancer agents. *J Mol Struct*, 1269 (2022) 133785.

43 Alghuwainem YAA, Abd El-Lateef HM, Khalaf MM, Abdelhamid AA, Alfarsi A, Gouda M, Abdelbaset M & Abdou A, Synthesis, structural, DFT, antibacterial, antifungal, anti-inflammatory, and molecular docking analysis of new VO(II), Fe(III), Mn(II), Zn(II), and Ag(I) complexes based on 4-((2-hydroxy-1-naphthyl)azo) benzenesulfonamide. *J Mol Liq*, 369 (2023) 120936.

44 Toppo AL, Yadav M, Dhagat S, Ayothiraman S & Eswari JS, Molecular docking and ADMET analysis of synthetic statins for HMG-CoA reductase inhibition activity. *Indian J Biochem Biophys*, 58 (2021) 127.

45 TrilaksanaH, Thanmayalaxmi D & Suvitha A, ADMET, pharmacokinetic and docking properties of the fungal drug 2-(2,4-difluorophenyl)-1,3-bis(1,2,4-triazol-1-yl)propan-2-ol by using quantum computational methods. *Indian J Biochem Biophys*, 60 (2023) 58.